

# Removal of heavy metals and bacteria from aqueous solution by novel hydroxyapatite/zeolite nanocomposite, preparation, and characterization

Mojgan Zendeheel<sup>1</sup> · Bahareh Shoshtari-Yeganeh<sup>1</sup> · Giuseppe Cruciani<sup>2</sup>

Received: 31 January 2016 / Accepted: 8 June 2016 / Published online: 20 June 2016  
© Iranian Chemical Society 2016

**Abstract** In this study, a HAp/NaP nanocomposite was prepared by adding a synthesized nano-hydroxyapatite to zeolite NaP gel in the hydrothermal condition and used for the removal of lead(II) and cadmium(II) ions from aqueous solution. HAp/zeolite nanocomposite was then characterized by Fourier transform infrared spectroscopy, X-ray diffraction and Rietveld method, scanning electron microscope, energy-dispersive X-ray analysis, and surface area and thermal analyses. Results suggested that the nanocomposite crystals of HAp were dispersed onto the zeolite external surface and/or encapsulated within the zeolite channels and pores. The potential of the composite in adsorption of heavy metals was investigated by using batch experiment. The metal concentration in the equilibrium  $C_e$  (mg/g) after adsorption with nanocomposite of HAp/NaP was analyzed using flame atomic adsorption spectrometry. The adsorption experiments were carried out at pH of 3–9. The influences of contact time, initial concentration, dose, and temperature on the adsorption of lead and cadmium ions were also studied. Results show that these nanocomposites have further adsorption related to NaP and HAp. They have great potential (about 95 %) for Pb(II) and Cd(II) adsorption at room temperature. The equilibrium process was described by Freundlich, Langmuir, Temkin, and Dubinin–Radushkevich (D-R) models. The kinetics data were successfully fitted by a pseudo-second-order model. The in vitro antibacterial activity of

these composites was evaluated against *Bacillus subtilis* (as Gram-positive bacteria) and *Pseudomonas aeruginosa* (as Gram-negative bacteria) and compared with standard drugs that show inhibition on bacterial growth.

**Keywords** Hydroxyapatite/zeolite · Heavy metal · Removal · Isotherm · Adsorption kinetics · Antibacterial activity

## Introduction

The pollution caused by toxic heavy metal ions such as Pb(II), Cd(II), and Zn(II) has become a highly harmful effect for animals, plants, and even humans because of their non-biodegradable properties and bioaccumulation in organisms [1]. Meanwhile, Pb(II) and Cd(II) have been classified as very toxic heavy metals. For instance, lead can destruct the nervous system, brain, liver, kidney, and reproductive systems [2]. Utilization of water containing very low concentration of Pb(II) ions for a long term causes several health problems such as coma, nausea, renal failure, and cancer [3]. It can be suggested that Pb(II) replaces calcium in the bones forming repository sites for long-term release [4]. cadmium has a severe toxicity and causes a wide range of health problems such as kidney disease, blood pressure, and reduction in red blood cells [5]. Therefore, removal of heavy metal ions from contaminated water is a very important aim for human health and environmental protection.

Several methods are presented for elimination of heavy metal ions from aqueous solution such as ion exchange, electrochemical treatment, chemical precipitation, reverse osmosis, and adsorption [6]. The researchers are interested in adsorption as an attractive technology due to high

✉ Mojgan Zendeheel  
m-zendeheel@araku.ac.ir

<sup>1</sup> Department of Chemistry, Faculty of Science, Arak University, Arak 38156-8-8349, Iran

<sup>2</sup> Department of Physics and Earth Sciences, University of Ferrara, Via G. Saragat 1, 44122, Ferrara, Italy

efficiency, simple process, and reduced cost [7]. Activated carbon, clays, and polymeric materials are considered as the usual adsorbents [8]. There are desirable properties for activated carbon, namely large surface area, extremely developed porosity, and high surface reactivity [9]. High production cost of this compound caused limitation in its application as adsorbent. Therefore, effort is still needed to exert more impressive adsorbents.

Zeolites are naturally occurring aluminosilicates which can be also obtained by synthesis and characterized by high internal and external surface areas. Several types of moieties such as water and alkaline/alkaline earth metals can be hosted or adsorbed in both natural and synthetic zeolites porous and channels. The NaP zeolite which has a gismondine (GIS) framework topology is a synthetic zeolite with two channels along [100] and [010] directions that both delimited by elliptical eight-membered tetrahedral rings with variable apertures depending on the framework flexibility of ( $3.1 \text{ \AA} \times 4.5 \text{ \AA}$ ) and ( $2.8 \text{ \AA} \times 4.8 \text{ \AA}$ ), respectively [10]. Literature reviews show that zeolites in general are very effective for the removal/immobilization of toxic and radioactive waste species, heavy metals and ammonium from wastewaters, and seawater potassium extraction, and also they apply for the production of environmentally friendly detergent [11].

Hydroxyapatite (HAp),  $\text{Ca}_{10}(\text{PO}_4)_6(\text{OH})_2$ , is a class of materials from different origins (mineral, synthetic, and derived from animal and fish bones) which has been used as sorbent of heavy metals such as Pb, Zn, Cu, Cd, and Co [12–15]. Recently, Ramesh et al. [16] have used a hydroxyapatite as an adsorbent in the removal of heavy metals in both single and binary systems. Corami et al. [17] studied the removal of copper and zinc by hydroxyapatite, while Sairam Sundaram et al. [18] have synthesized nano-hydroxyapatite and tested it for the removal of fluoride. Dancuet al. and Lin et al. used HAp in the removal of nicotinic acid and phenol, respectively [19]. Besides, HAp special in nanoform has high biocompatibility and bioactivity properties [20].

Herein, we report the synthesis and characterization of hydroxyapatite/NaP nanocomposite. It explored the possibility of using this composite as an adsorbent for efficient removal of Pb(II) and Cd(II) from aqueous solution. The nanocomposite adsorbent was characterized by X-ray diffraction (XRD), Fourier transform infrared (FT-IR) spectroscopy, scanning electron microscopy (SEM), energy-dispersive X-ray analysis (EDAX), surface area measurements (BET), and thermogravimetric analyses (TGA). The adsorption of Pb(II) and Cd(II) on HAp/NaP was also investigated through batch experiments. To obtain the optimized condition for application of this compound as adsorbent, we studied different parameters such as contact time, pH, initial metal ion concentration, and the dose of

adsorbent. Moreover, different adsorption isotherms (Freundlich, Langmuir, Temkin, and Dubinin–Radushkevich) were evaluated. The adsorption kinetic parameters were determined to obtain the adsorption capacity for lead and cadmium solutions. Finally, in vitro antibacterial activity of these nanocomposites was evaluated against *Bacillus subtilis* (as Gram-positive bacteria) and *Pseudomonas aeruginosa* (as Gram-negative bacteria) via utilizing the agar disc diffusion method under anaerobic conditions and compared with standard drugs.

## Materials and methods

### Materials

The starting materials such as silica gel, sodium hydroxide, aluminum hydroxide, calcium nitrate (CNT), potassium dihydrogen phosphate (KPP), ammonia, sulfuric acid ( $\text{H}_2\text{SO}_4$ ), and deionized water were used in this study (all chemical materials supplied by Merck).

### Characterization techniques

The preliminary XRD identification of crystalline phases was carried out by a Philips X'Pert diffractometer operating with Cu-K $\alpha$  radiation. XRD patterns with better statistics were also collected on the HAp/NaP nanocomposite with 1:1 molar ratio of HAp and NaP using a Bruker D8 Advance diffractometer with an X-ray tube operating at 40 kV and 40 mA and equipped with a Si(Li) solid-state detector (Sol-X) set to measure Cu-K $\alpha_{1,2}$  radiation. Measuring conditions were 5–95° range, 0.02° scan step, and counting time per step is 4 s. Rietveld refinement of this diffraction pattern was performed by the TOPAS v.4.1 program (Bruker AXS). The crystallite size of NaP and HAp in the composite was determined by the Double-Voigt approach as implemented in TOPAS. In particular, the crystallite size was calculated as volume-weighted mean column heights based on integral breadths of peaks.

FT-IR spectra were recorded by a Galaxy series FT-IR 5000 spectrometer. TG/DTA curves were measured by a Diamond TG/DTA PerkinElmer thermoanalyzer. SEM images were acquired by a Philips XL30 electron microscope. BET was recorded by Belsorp mini II.

### Preparation of HAp

Syntheses of hydroxyapatite powder were done according to the following procedure: 0.05 mol (1 M) of CNT and 0.03 mol (0.6 M) of KPP were completely dissolved in 50 mL of deionized water at ambient temperature. The

solution of CNT was added slowly to the KPP solution. The pH value was adjusted to 11 by ammoniac solution. The reaction mixture was stirred 1 h and then kept for 24 h to complete the reaction. The final milky suspension was then filtered off and washed two times with hot water for the removal of residual potassium, ammonium, and nitrate ions. This product was dried at 40 °C for 24 h. The precipitate was calcinated at 600 °C for 1 h.

### Preparation of HAp/NaP composite

Various aliquots (0.175, 0.350, and 0.700 g) of the prepared hydroxyapatite were initially added to a zeolite gel. For the preparation of the zeolite gel, the following procedure was applied: To an Erlenmeyer flask on the stirrer, 16.13 g of sodium silicate (containing 19.8 wt% SiO<sub>2</sub>), 6 mL of initiator, 13.2 mL of sodium hydroxyl (24 wt%), and 5.2 g of deionized water were added. The stirring of this reaction has been continued for 15 min. The mixtures were then placed in an autoclave at 100 °C for 26 h. The three composites with different ratios of HAp/zeolite gel (0.5:1, 1:1, and 2:1) were synthesized and then filtered and washed with deionized water repeatedly in order to reach pH of 7. Gel-like products were dried at ambient temperature to yield white powders, and then they were used as adsorbents for the removal of Pb(II) and Cd(II) from aqueous solutions in the batch mode experiment.

### Adsorption studies

The bath adsorption experiment of lead(II) and cadmium(II) from single aqueous solutions was performed. 2 g/L of adsorbent was contacted with 25 mL of metal solution with desired concentration, pH, and temperature. To achieve saturated adsorption, the sample solution was shaken for 2 h at ambient temperature, and then, the solid was separated from the solutions and the concentration of the residue Pb(II) and Cd(II) was determined by a PerkinElmer Analyst 2380 AAS.

The adsorption capacity of lead(II) and cadmium(II) ions (mg/L) on to the HAp/NaP was calculated according to the following equation:

$$q_e = \frac{(C_0 - C_e)V}{W} \quad (1)$$

where  $C_0$  and  $C_e$  are the initial and equilibrium concentration (mg/L) of lead(II) or cadmium(II) ions, respectively. Also,  $q_e$  (mg/g) is the amount of adsorbate adsorbed per unit mass of adsorbent,  $V$  is the volume solution (in liter), and  $W$  is the weight of HAp/NaP nanocomposite (in grams).

The removal efficiency of metal ions from aqueous solution (in percent) was calculated by the following equation:

$$\% \text{Removal} = \frac{C_0 - C_e}{C_0} \times 100 \quad (2)$$

### Antibacterial activity study

The in vitro antibacterial activity of the investigated compounds was tested against pathogenic Gram-negative bacteria such as *P. aeruginosa* (ATCC 27853) and Gram-positive bacteria such as *B. subtilis* (ATCC 6633) using the paper disc diffusion method according to the procedure described by Hwang and Ma [21]. This method is a way to measuring efficiency of an antibacterial agent against the mentioned bacterial growth. Muller Hinton broth was used for preparing culture media for the bioassay of the organisms. A lawn culture from 0.5 Mac Farland suspension of each strain was prepared on Muller Hinton agar. The agar medium was sterilized in autoclave and cooled to room temperature, and then introduce into sterilized petri dishes. The bacteria are swabbed uniformly across a culture plate, while the petri dishes are cooled over 24 h. Discs of samples were placed on the surface of the medium, and finally, all petri dishes containing bacteria and antibacterial reagents were incubated and maintained at 37 °C for 24 h. The diameters of the inhibition zones formed around each disc were determined and presented in mm.

### Results and discussion

Table 1 shows the effect of hydroxyapatite dose on removal of lead(II) and cadmium(II). HAp/NaP nanocomposite with 1:1 molar ratio of HAp to NaP shows the best result for the adsorption of heavy metals. Therefore, this sample was selected for the examined characterizations.

**Table 1** Effect of hydroxyapatite dose on removal of lead(II) and cadmium(II)

Hydroxyapatite (g)	Pb(II) (removal %) 2 h/pH = 5/25 ppm/0.05 g/25 °C	Cd(II) (removal %) 2 h/pH = 8/5 ppm/0.05/25 °C
0.175	%R = 59.64	%R = 42.6
0.350	%R = 98	%R = 99.96
0.700	%R = 69.6	%R = 62.3

### FT-IR analysis

The FT-IR spectrum of the nanocomposite of NaP, HAp/NaP, and HAp is revealed in Fig. 1. The positions of the significant absorption bands for the NaP zeolite are as follows: 3466, 1653, 1012, 799, and 437  $\text{cm}^{-1}$ . The bands at 3466 and 1653  $\text{cm}^{-1}$  can be attributed to the hydroxyl group stretching vibration and H–O–H bending vibration, respectively [22]. The band at 1012  $\text{cm}^{-1}$  is related to internal tetrahedral asymmetrical stretching, and the band at 799 and 437  $\text{cm}^{-1}$  is ascribed to amorphous  $\text{SiO}_2$  stretching vibration and  $\text{TO}_4$  (T=Si, Al) bending mode, respectively [23]. There are eight main absorption bands for hydroxyapatite at 3574, 1456, 1035, 962, 854, 601, 567, and 474  $\text{cm}^{-1}$ . The peak at 3574  $\text{cm}^{-1}$  is assigned to the stretching vibration of OH in hydroxyapatite lattice. Two peaks at 1456 and 854  $\text{cm}^{-1}$  are assigned to carbonate group. The band

at 1035  $\text{cm}^{-1}$  is attributed to P=O stretching vibration of  $\text{PO}_4^{3-}$ . The band at 962  $\text{cm}^{-1}$  is attributed to symmetric P=O stretching vibration ( $\nu_1$ ). The bands at 567 and 601  $\text{cm}^{-1}$  are ascribed to the  $\nu_4$  bending vibration of phosphate group, and the 474  $\text{cm}^{-1}$  band resulted from the  $\nu_2$  phosphate mode [24]. Finally, in the spectrum of composite, the bands at 3480 and 1653  $\text{cm}^{-1}$  are attributed to the OH stretching and bending vibration, respectively. The peak at 1030  $\text{cm}^{-1}$  is related to the P=O stretching vibration of  $\text{PO}_4^{3-}$ . The band at 742  $\text{cm}^{-1}$  is attributed to amorphous  $\text{SiO}_2$  stretching vibration. The band at 605  $\text{cm}^{-1}$  is assigned to the bending vibration of phosphate group, and the band at 435  $\text{cm}^{-1}$  is ascribed to the  $\text{TO}_4$  (T=Si or Al) bending mode [23]. It is clear that the FT-IR spectrum of HAp/NaP nanocomposite shows both the characteristic absorption bands of hydroxyapatite and NaP zeolite. These results suggested the presence of HAp and NaP phases in the product.

**Fig. 1** FT-IR spectra of NaP (a), HAp/NaP nanocomposite (b), and hydroxyapatite (c)

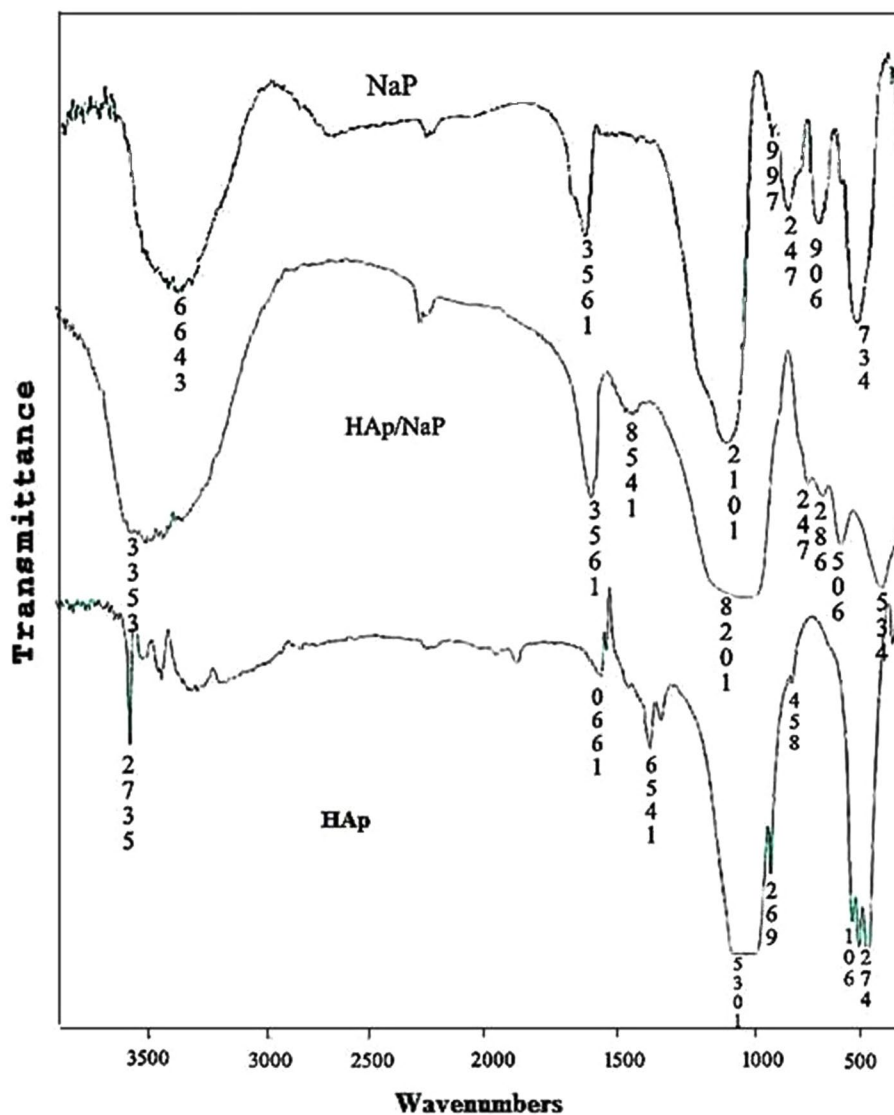
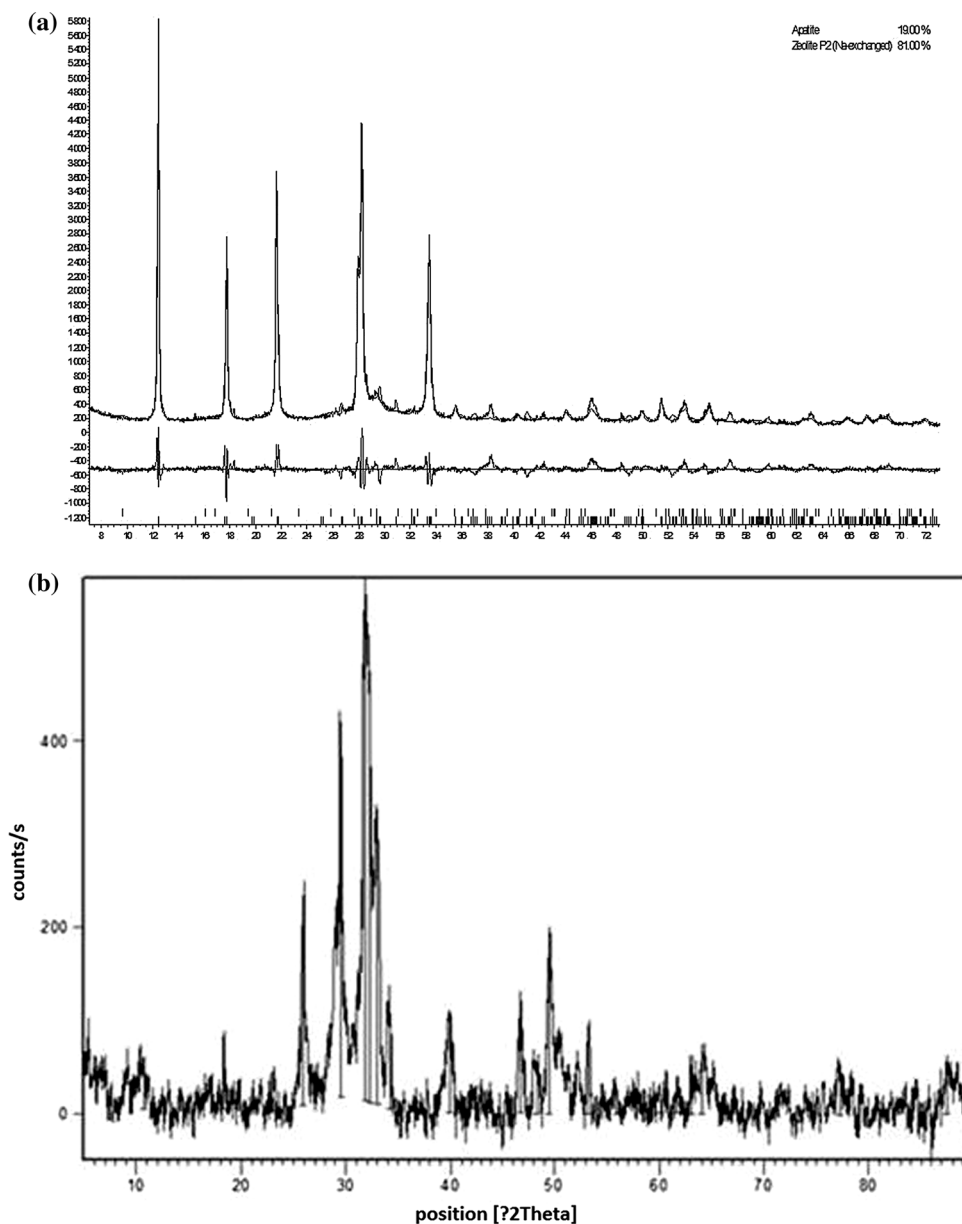


**Fig. 2** **a** Rietveld fit of XRD pattern of HAp/NaP nanocomposite, **b** XRD pattern of HAp/NaP nanocomposite with 3:1 ratio



## XRD

Besides the preliminary XRD analysis for phase identification, a diffraction pattern with better statistics was collected and fitted by the Rietveld method (Fig. 2a) in order to determine some structural and microstructural features of the HAp/NaP nanocomposite. The most intense characteristic XRD peaks of NaP zeolite at  $2\theta = 12.48^\circ$ ,  $17.92^\circ$ ,  $21.79^\circ$ ,  $28.10^\circ$ , and  $33.40^\circ$  are clearly visible, showing that a relatively well-crystallized gismondine-like zeolite has been obtained by synthesis and preserved in the HAp/NaP composite. On the contrary, only very broad and weak diffracted peak at about  $2\theta = 29^\circ$  can be attributed

to hydroxyapatite [25]. This is consistent with the very low loading of HAp in the composite (below 50 mg in 1 g of zeolite) and the very small nanosize of HAp which could also be incorporated into the zeolite pores in agreement with what reported by other researchers [26, 27]. Rietveld fit for HAp/NaP nanocomposite showed that the gismondine-like zeolite structure can be successfully modeled based on the crystal structure model of synthetic Na-exchanged P2 by Hansen et al. [28] in the orthorhombic *Pnma* space group. Refined unit cell parameters are as follows:  $a = 9.957(1) \text{ \AA}$ ,  $b = 9.978(1) \text{ \AA}$ ,  $c = 10.093(1) \text{ \AA}$ . The Rietveld fits confirm that the broad diffraction peak around  $2\theta = 29^\circ$  is consistent with the occurrence of

nano-hydroxyapatite (crystallite size  $\sim 8$  nm), modeled on the basis on the hydroxyapatite crystal structure model of El Feki et al. [29] in the  $P6_3/m$  space group with refined unit cell parameters:  $a = 10.53(1)$  Å,  $c = 6.88(1)$  Å. For further considerations, we investigated XRD pattern for HAp/NaP nanocomposite with 4:1 ratio that in addition to NaP peaks (Fig. 2b), the main peaks related to the hydroxyapatite at  $2\theta = 12.63^\circ, 18.44^\circ, 21.80^\circ, 28.43^\circ, 29.52^\circ, 44.27^\circ, 46.12^\circ, 48.62^\circ, 50.12^\circ$  are attributed. So this indicates the presence of crystalline HAp and NaP zeolite in the composite.

### SEM

The morphologies of obtained product were observed by electron microscopy. Figure 3a–d shows SEM images of

HAp/NaP nanocomposite and hydroxyapatite. SEM image of HAp/NaP composite (Fig. 3a, b) clearly indicates the presence of both the cactus-like and diamond-like morphologies. These morphologies show the NaP phase in the composite, and it is similar to what previously reported [30] and the size of diamond-shape particle is about  $1\text{--}2$   $\mu\text{m}$ . Figure 3c, d shows that the particle size of HAp in the composite is about  $40\text{--}70$  nm. It could be explained that the zeolite network might have possibly acted as a dispersing agent for the hydroxyapatite nanocrystals over the external surface of the zeolite crystals and/or into the NaP zeolite pores.

Figure 4a, b shows the EDAX spectra of HAp and HAp/NaP nanocomposite, respectively. The detected atomic Ca/P ratio for the pure HAp sample is 1.55 which is in the range of ideal stoichiometric hydroxyapatite. As shown in

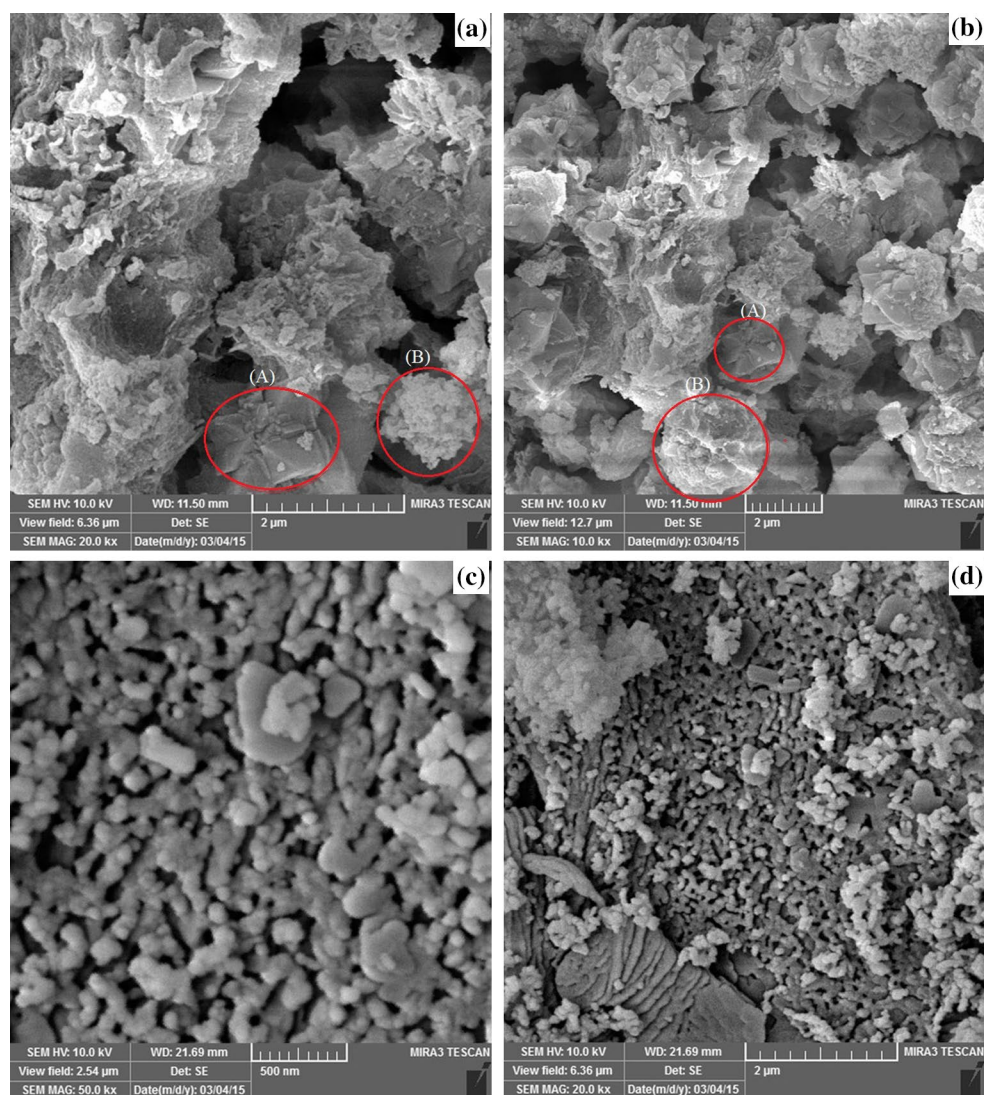


**Fig. 3** SEM micrograph of **a, b** HAp/NaP nanocomposite and **c, d** HAp

**Fig. 4** **a** EDAX spectra of the hydroxyapatite, **b** HAp/NaP nanocomposite

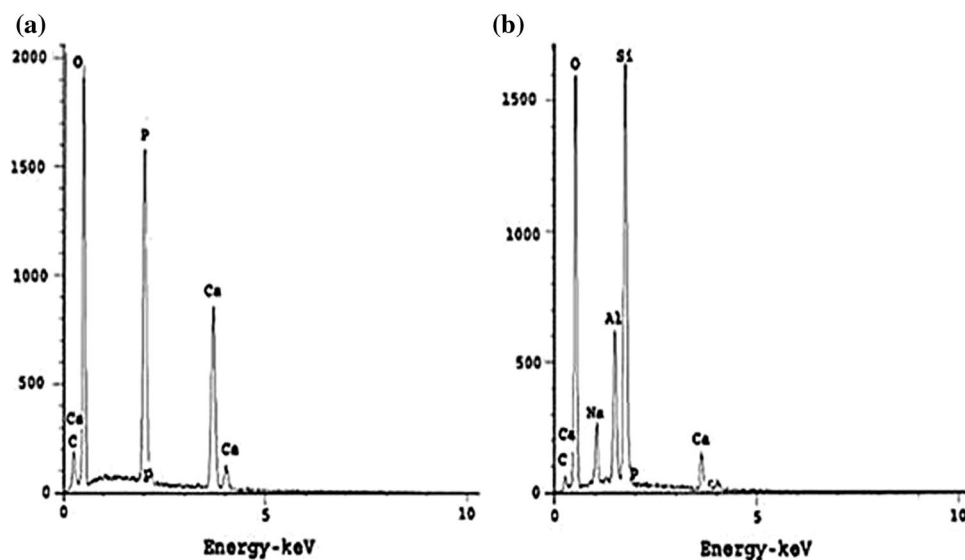


Fig. 4b, the presence of Si, Al, and Na is clearly attributable to the NaP zeolite, whereas the minor presence of Ca and P can be related to hydroxyapatite. It is consistent with the small HAp/NaP ratio and the possible encapsulation of HAp nanocrystals into the zeolite pores [26, 27].

Also, it seems that the fine dispersion of HAp by considering the XRD and SEM in lower ratio without significant aggregation of HAp nanocrystallites that may cause the 1:1 molar ratio of HAp to NaP was the best ratio for the adsorption of heavy metals.

## BET

### Nitrogen adsorption–desorption

The specific surface areas and pore volume of the adsorbent were estimated by nitrogen adsorption at relative pressures ( $P/P_0$ ) in the range of 0.008–0.5. The BET data for the NaP zeolite after loading of hydroxyapatite show a small decrease from 45 to 35.62  $\text{m}^2/\text{g}$ . Since the zeolite framework structure is not affected by incorporated HAp as shown by the XRD pattern and SEM, the reduction in surface area and pore volume provides the presence of HAp in the cavities [31].

The  $\text{N}_2$  adsorption/desorption isotherms of as-synthesized materials are given in Fig. 5. These isotherms can be classified as type I characteristic of the microporous materials [32, 33].

### Thermal analysis

The TG-DSC curves of the NaP zeolite demonstrated two mass loss steps for NaP zeolite (Fig. 6a). The first loss of about 10 % in the temperature range 25–200 °C, associated

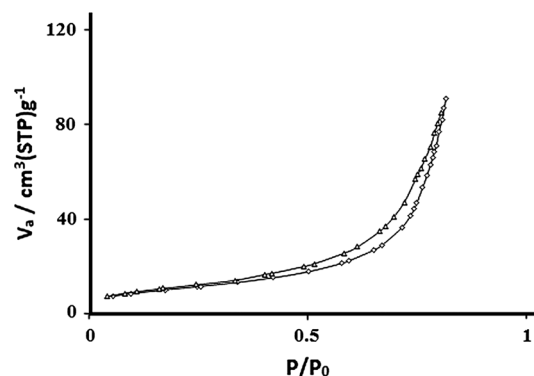


**Fig. 5** Adsorption/desorption isotherm of HAp/NaP nanocomposite

with an endothermic DTA peak, can be ascribed to release of water. The second event with loss of about 4.1 % in the temperature range 200–400 °C can be attributed to the removal of hydroxyl groups. A third step marked by weak endothermic peaks in the temperature range 400–700 °C might be related to some phase transformations which are known to occur in gismondine-like structures [30, 34, 35].

TG/DTA curves of HAp/NaP nanocomposite adsorbent were recorded at 10 °C/min in inert atmosphere over a temperature range of 30–900 °C (Fig. 6b). The 11.85 % weight loss in the first region can be attributed to the adsorbed water in zeolite NaP (30–200 °C). The 5.06 % weight loss in the second step (200–500 °C) may be assigned to both the removal of the hydroxyl group of zeolite and condensation of the hydrogen phosphate groups to form pyrophosphates ( $\text{P}_2\text{O}_7^{2-}$ ) in the hydroxyapatite. The weight loss about 4.65 % occurring in the last step at about 800 °C can be ascribed to the phase transformation of zeolite and the conversion of  $\text{P}_2\text{O}_4^{4-}$  to form  $\text{PO}_4^{3-}$  [36, 37].

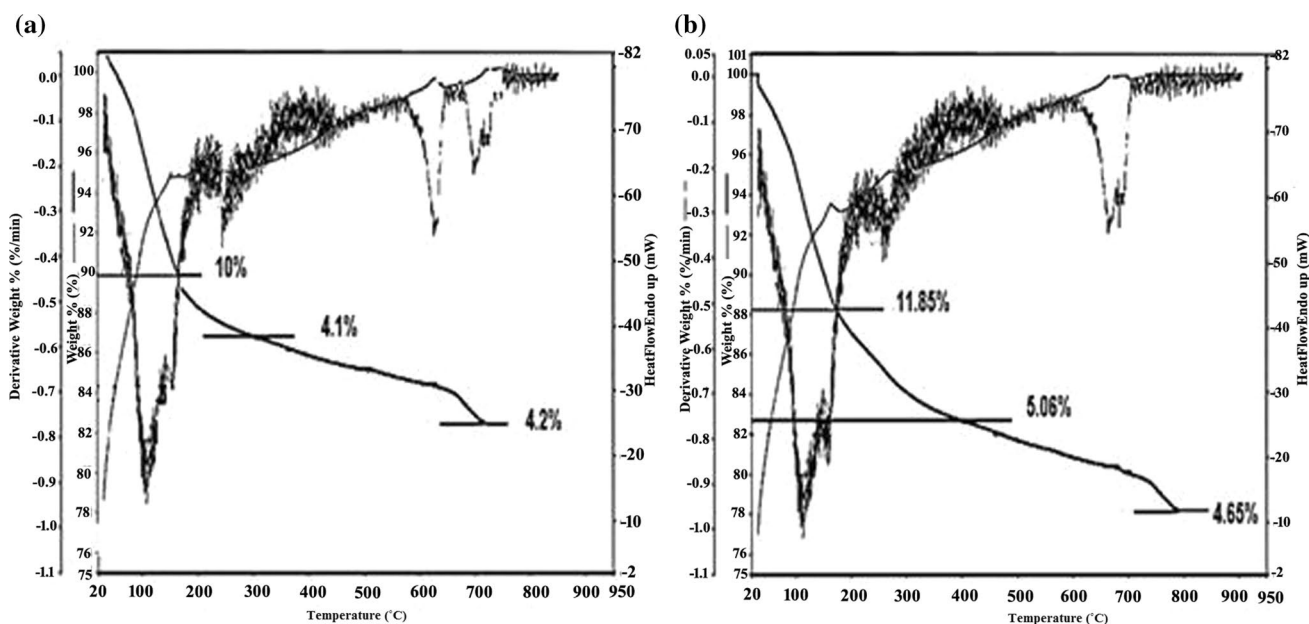


**Fig. 6** a TG/DTG/DTA curves of NaP, b HAp/NaP nanocomposite

## Batch experiments

### Effect of contact time

The effect of contact time on percentage removal of lead(II) and cadmium(II) from aqueous solution was studied in the different time ranging from 30 min to 24 h. The initial metal concentration of 100 ppm for each solution and pH of 6 were used according to other works [4, 38]. After pre-defined contact time, the adsorbent was separated and the residual metal concentration was analyzed. The effect of contact time on Pb(II) and Cd(II) adsorption efficiency is shown in Fig. 7a. It can be observed that the rate of removal of Pb(II) and Cd(II) ions was higher at the initial stage, very likely due to the availability of more active sites on the surface of nanocomposite. It became slower at the later stages of contact time, due to the decreased number of active sites [2]. It is clear from Fig. 7a that up to 12 h, the removal efficiency was very high reaching 95 % and further increase in contact time did not significantly reduced the ion removal. However, the contact time of 2 h was considered as the equilibrium time for maximum adsorption. The initial faster rate may be attributed to the availability of the uncovered surface area of the HAp/NaP nanocomposite, since the adsorption kinetics depends on the surface area of the adsorbents. The metal ion adsorption takes place at the more reactive sites. As these sites are increasingly filled, the sorption process becomes less favored [39].

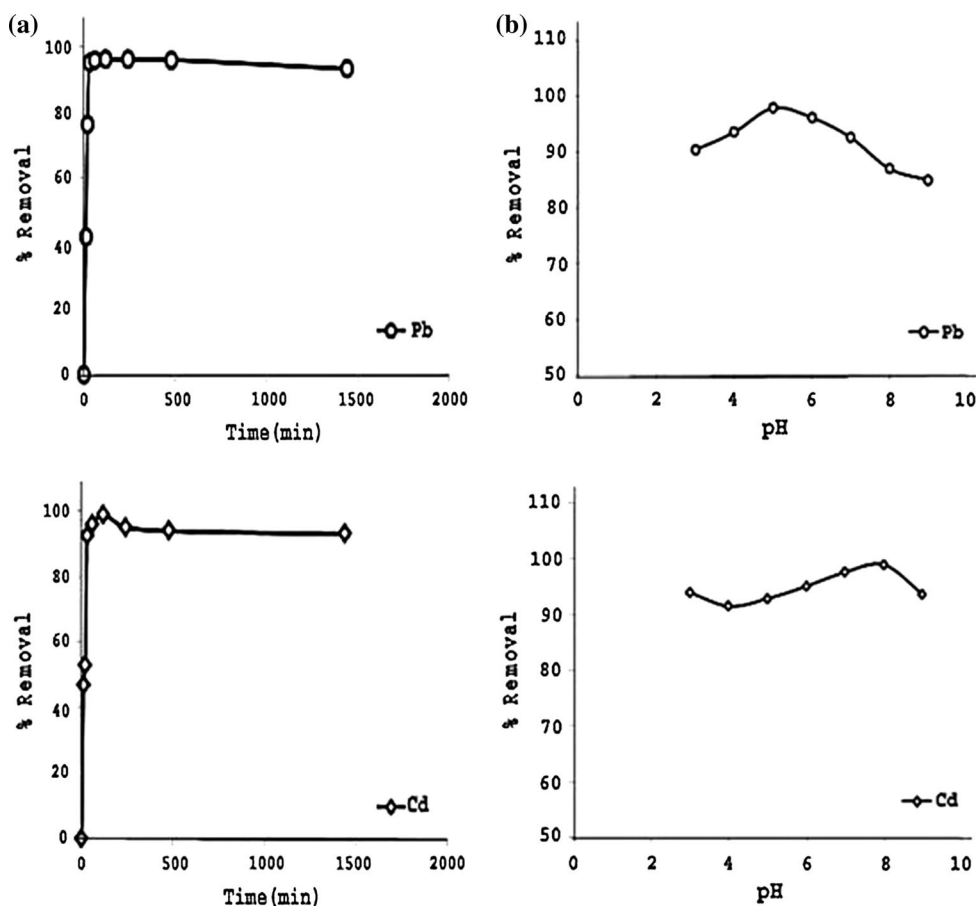
### Effect of pH

The adsorption of lead(II) and cadmium(II) on HAp/NaP as a function of initial pH in optimized reaction conditions (contact time, initial metal concentration, amount of HAp/NaP, and temperature) was analyzed by adjusting the pH of the aqueous solution at rang of 3–9 with HNO<sub>3</sub> (0.1 N) or NaOH (0.1 N). After 2 h, the suspension was filtered and the residual concentration of metal ions was evaluated. From Fig. 7b, it was found that the maximum adsorption with % R = 97.8 and % R = 98.8 is achieved at pH of 5 for Pb(II) and pH of 8 for Cd(II), respectively. Thus, pH of 5 and 8 for these ions was taken into consideration for further investigations. The HAp was not dissolute from the zeolite at the low pH. For this purpose, we investigated the FT-IR and XRD of adsorbent after treatment with acid, and there were not any drastic changes in the spectrum and they were like fresh adsorbent.

Figure 7b shows that the Pb(II) adsorption capacity for HAp/zeolite increases slightly with increasing initial pH from 3 to 5, but it decreases continuously with increasing pH from 5 to 9. This indicates that the Pb(II) adsorption capacity for HAp/zeolite in acidic solution is better than neutral or alkaline solution. According to the literature, at low pH (<6) the positively charged Pb(II) species are dominant and adsorption on nanocomposite takes place in faster rate. There are several lead species with different charges in the higher pH values (6–9) like Pb(OH)<sup>+</sup>



**Fig. 7** **a** Effect of contact time on the amount of removal of heavy metals adsorbed on HAp/NaP. **b** The effect of pH value on the amount of removal of heavy metals adsorbed on HAp/NaP



and  $\text{Pb}(\text{OH})_2$ . Thus, the removal of lead in these pH ranges is possibly accomplished by simultaneous precipitation of  $\text{Pb}(\text{OH})_2$  and sorption of  $\text{Pb}(\text{OH})^+$  [2]. In case of  $\text{Cd}(\text{II})$ , adsorption capacity decreased slightly with increasing pH from 3 to 5, but it increased continuously with increasing pH from 5 to 8, and then, a decreasing pH of 9 was observed. So these results indicate that the  $\text{Cd}(\text{II})$  adsorption capacity in alkaline solution is better than in acidic solution. The growth in  $\text{Cd}(\text{II})$  removal with increasing pH can be explained on the basis of a decrease in competition between proton and  $\text{Cd}(\text{II})$  for the surface sites and so the decrease in the positive surface charge, which results in a lower coulombic repulsion of the sorbing  $\text{Cd}(\text{II})$  [40].

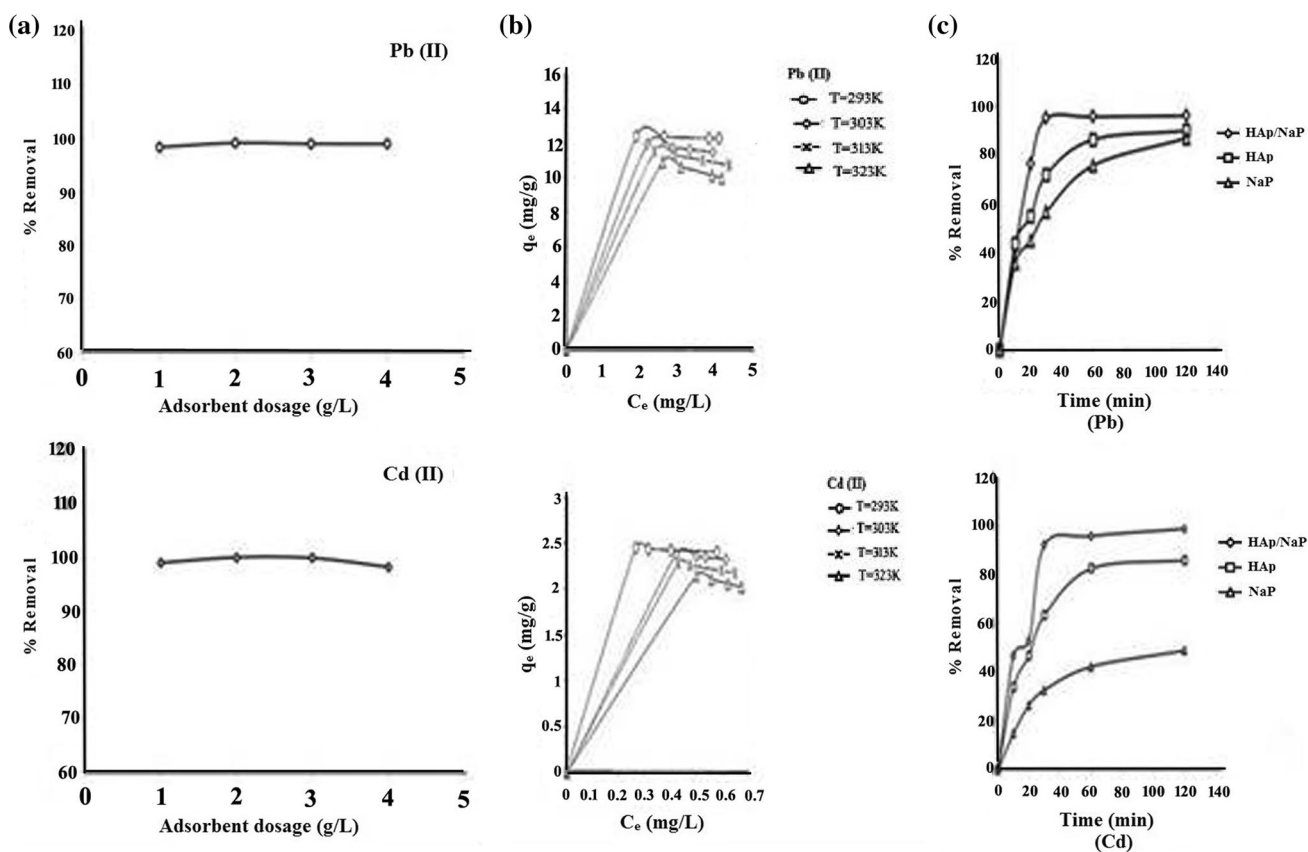
#### Adsorbent dose

Figure 8a shows the effect of adsorbent dose on removal of  $\text{Pb}(\text{II})$  and  $\text{Cd}(\text{II})$  from aqueous solution. The tests were made by various adsorbent doses of 1, 2, 3, and 4 g/L. Other parameters such as initial concentration, contact time, pH, and temperature were maintained constant and based on the obtained optimum conditions in previous sections. As it is shown in Fig. 8b, there was no significant

change in adsorption removal efficiency by using different dose of adsorbent. However, increment of HAp/NaP amount provides greater sorption sites while a large amount of the adsorbent effectively reduces the unsaturation of such sites of per unit mass, resulting in the great reduction in per unit mass adsorption at higher HAp/NaP amount [41]. Thus, the dose of 2 g/L, which gave maximum metal ion removal, was taken into consideration for further experiments.

#### Effect of temperature

To study the temperature effect on  $\text{Pb}(\text{II})$  and  $\text{Cd}(\text{II})$  adsorption, the adsorption of  $\text{Pb}(\text{II})$  and  $\text{Cd}(\text{II})$  solution in optimum condition was examined at four temperatures 20, 30, 40, and 50 °C. As shown in Fig. 8b, it was found that by increasing the temperature from 20 to 50 °C, the maximum adsorption capacity decreased. This indicates that the adsorption of  $\text{Pb}(\text{II})$  and  $\text{Cd}(\text{II})$  by HAp/NaP nanocomposite is an exothermic process [34]. This was further supported by calculating thermodynamic parameters such as free energy change ( $\Delta G$ ), enthalpy change ( $\Delta H$ ), and entropy change ( $\Delta S$ ). These parameters were calculated using the following equation [42]:



**Fig. 8** a Effect of adsorbent dosage on the removal of Pb(II) and Cd(II), b Effect of temperature on the adsorption of Pb(II) and Cd(II) to HAp/NaP. c The comparison of HAp/NaP with HAp and zeolite as an adsorbent for the removal of Pb(II) and Cd(II)

$$\text{Log } K_c = \frac{\Delta S}{2.303R} - \frac{\Delta H}{2.303RT} \quad (3)$$

$$\Delta G = \Delta H - T\Delta S \quad (4)$$

where  $\Delta H$  and  $\Delta S$  are the change in enthalpy and entropy of adsorption, respectively, and  $R$  refers to the universal gas constant (8.314 kJ/mol K).  $K_c$  value is the equilibrium constant and calculated from Langmuir isotherm. Values of  $\Delta H$  and  $\Delta S$  were calculated from the slope and intercept of Vant Hoff plot ( $\text{Log } K_c$  versus  $1/T$ ) and represented in Table 2. The Gibbs free energy change values in each temperature were found as negative, which indicated the spontaneity and feasibility of the adsorption. The negative value of enthalpy indicates the exothermic process of adsorption. The positive value of  $\Delta S$  suggests that the entropy is responsible for making the  $\Delta G$  negative value. So the adsorption process was spontaneous.

#### Effect of type of adsorbent

The influence of the type of adsorbent was investigated in the presence of HAp/NaP nanocomposite, hydroxyapatite

**Table 2** Thermodynamic parameters of HAp/NaP nanocomposite in the removal of Pb(II) and Cd(II)

Temperature (K)	$\Delta G^\circ$ (Kj mol <sup>-1</sup> )	
	Pb(II)	Cd(II)
293	-19.147	-17.89
303	-20.33	-19.56
313	-20.36	-21.19
323	-28.52	-21.33
$\Delta H^\circ$ (K j mol <sup>-1</sup> )	-72.997	-15.953
$\Delta S^\circ$ (j mol <sup>-1</sup> K <sup>-1</sup> )	311.1	116.71

and zeolite NaP single components for the removal of lead and cadmium ions. These tests were studied in the obtained optimized conditions (time, pH, temperature, and adsorbent dosage). As shown in Fig. 8c, the removal of both ions with HAp/NaP nanocomposite was higher than hydroxyapatite and zeolite NaP adsorbents. The literature review showed that hydroxyapatite and zeolite NaP were found to be useful for heavy metal removal. HAp had better performance for water treatment due to its greater retention of heavy metals, its lower solubility in a wide range of pH, and the different

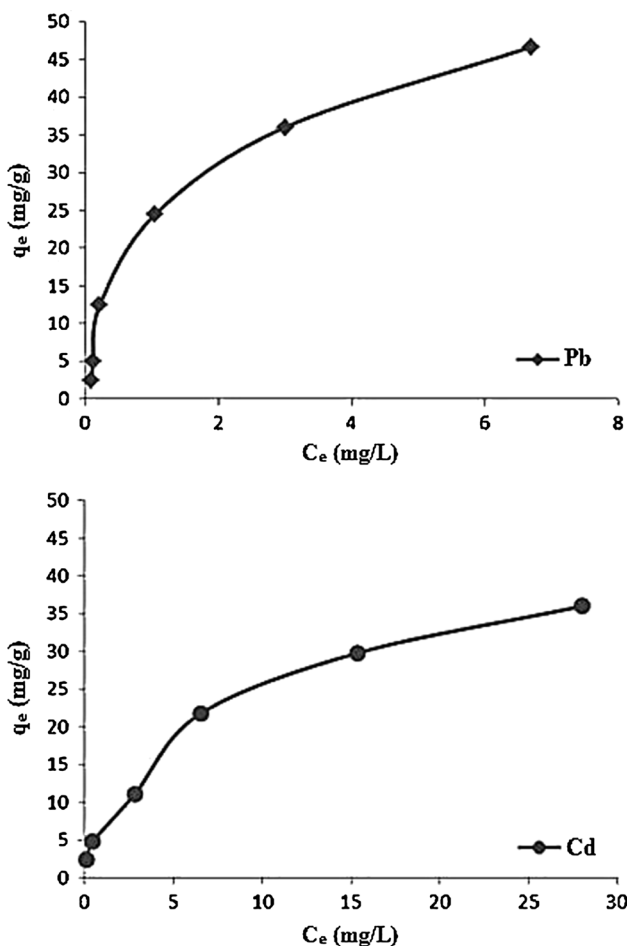


**Fig. 9** Adsorption isotherm for metal ion adsorption on HAp/NaP at optimum conditions

active mechanisms for the removal of metal cations such as ion exchange processes, adsorption, and dissolution/precipitation. Nevertheless, it seems that HAp does not regenerate and it is not recoverable [6]. According to the obtained results in Fig. 8c, it is very likely that coupling the relative merits of zeolite adsorbents (large surface area) with those of HAp listed above causes to HAp/NaP nanocomposite that is a very performing adsorbent for removal of heavy metals in comparison with only the zeolite and HAp.

*Adsorption isotherms*

Adsorption experiments for equilibrium process study were done under derived optimum experimental parameters for each metal ion solution. Figure 9 shows the relationship between the ions adsorbed per unit mass of adsorbent and its present concentration in solutions. It indicates that the composite of HAp/NaP is a suitable adsorbent for removing Pb(II) and Cd(II) from aqueous solutions, and it exhibited higher adsorption capacity for Pb(II) than Cd(II) in solutions.

Equilibrium relationships between adsorbent and adsorbate can be described by several models. Experimental models can be used to determine the design of adsorption. The empirical data obtained in the present work were examined by the Freundlich, Langmuir, Temkin, and Dubinin–Radushkevich isotherms. The linear form of Freundlich isotherm equation is given by Eq. 5:

$$\ln q_e = 1/n_f C_e + \ln K_f \tag{5}$$

where  $C_e$  and  $q_e$  are the equilibrium concentration of metal ions in the liquid phases ( $\text{mg L}^{-1}$ ) and adsorbed concentration ( $\text{mg g}^{-1}$ ), respectively.  $K_f$  and  $n_f$  are Freundlich constants, while  $K_f$  ( $\text{mg g}^{-1}$ ) is related to the bonding energy and  $n_f$  gives an indication of how desirable the adsorption process. The forms of Langmuir and the other isotherms are given in Table 3 [43].

In the equations in Table 3,  $q_m$  is the maximum sorption capacity ( $\text{mg g}^{-1}$ ),  $K_L$  Langmuir constant is related to energy of adsorption ( $\text{L mol}^{-1}$ ),  $A_T$  and  $b_T$  are Temkin isotherm constant,  $B_D$  is Dubinin–Radushkevich isotherm constant, and also  $q_D$  is Dubinin–Radushkevich isotherm constant ( $\text{mmol g}^{-1}$ ).

The Freundlich isotherm can be applied to describe the multilayer adsorption on the heterogeneous surface, and Langmuir model is the best known isotherms to describe the monolayer adsorption on the homogeneous surface. The derivation of the Temkin isotherm assumes that the fall in the heat of sorption is linear rather than logarithmic, as implied in the Freundlich equation. Finally, the other adsorption isotherm, the Dubinin–Radushkevich model (D-R), was applied to calculate adsorption data for the

**Table 3** Isotherm constants for two-parameter models by linear regression

Isotherm	Form	Plot	Slope intercept
Langmuir	$\frac{C_e}{q_e} = \frac{C_e}{q_m} + \frac{1}{q_m K_L}$	$C_e/q_e$ versus $C_e$	$\frac{1}{q_m} \quad \frac{1}{q_m K_L}$
Temkin	$q_e = RT/b_T \ln(A_T C_e)$	$q_e$ versus $\ln C_e$	$RT/b_T \quad RT \ln(A_T)/b_T$
Dubinin–Radushkevich	$q_e = q_D \exp(-B_D [RT \ln(1 + 1/C_e)]^2)$	$\ln q_e$ versus $(\ln(1 + 1/C_e))^2$	$-B_D \quad R^2 T^2 \ln(q_D)$

determination of the adsorption process nature (chemical or physical adsorption) [44]. The obtained parameters of all isotherm models for adsorbed Pb(II) and Cd(II) on the

**Table 4** Isotherm parameters for sorption of Pb(II) and Cd(II) by HAp/NaP

Isotherm	Pb(II)	Cd(II)
Freundlich	$n_f = 1.629$ $K_f = 18.5079$ ( $\text{mg g}^{-1}$ ) $R^2 = 0.8941$	$n_f = 2.047$ $K_f = 7.530$ ( $\text{mg g}^{-1}$ ) $R^2 = 0.9923$
Langmuir	$q_m = 55.55$ ( $\text{mg g}^{-1}$ ) $K_L = 0.747$ ( $\text{L g}^{-1}$ ) $R^2 = 0.9762$	$q_m = 40.16$ ( $\text{mg g}^{-1}$ ) $K_L = 0.229$ ( $\text{L g}^{-1}$ ) $R^2 = 0.9638$
Temkin	$b_T = 247.37$ $A_T = 14.253$ ( $\text{L mol}^{-1}$ ) $R^2 = 0.9932$	$b_T = 410.44$ $A_T = 7.4939$ ( $\text{L mol}^{-1}$ ) $R^2 = 0.8965$
Dubinin–Radushkevich	$q_D = 34.9808$ ( $\text{mg g}^{-1}$ ) $K_D = 0.0676$ ( $\text{mol}^2 \text{Kj}^{-2}$ ) $E = 2.72$ ( $\text{Kj mol}^{-1}$ ) $R^2 = 0.979$	$q_D = 19.3791$ ( $\text{mg g}^{-1}$ ) $K_D = 0.0632$ ( $\text{mol}^2 \text{Kj}^{-2}$ ) $E = 2.84$ ( $\text{Kj mol}^{-1}$ ) $R^2 = 0.7134$

HAp/NaP nanocomposite along with coefficient correlation ( $R^2$ ) are shown in Table 4.

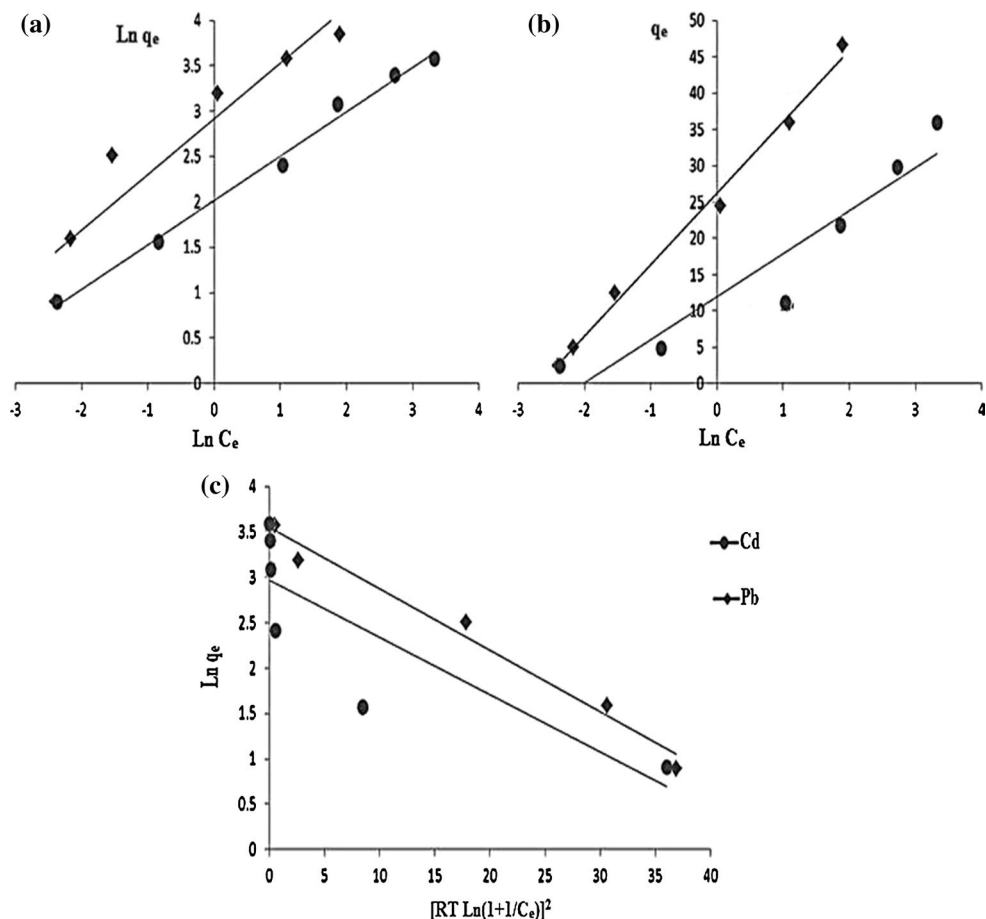
The plot of  $\text{Ln } q_e$  versus  $\text{Ln } C_e$  is illustrated in Fig. 10a. Based on the value of the correlation coefficient ( $R^2$ ), the Freundlich model gave a much better fit to the experimental data in Cd(II) in comparison with Pb(II) ion solution. Figure 11 shows that the experimental data for the removal of Pb(II) and Cd(II) ions were fitted by a Langmuir model for the studied concentration with a satisfactory agreement factor of regression ( $R^2$ ). Figure 10b shows the fitting plot of Temkin adsorption of Pb(II) and Cd(II) onto HAp/NaP composite. The plot of  $\text{Ln } q_e$  versus  $\varepsilon^2$  ( $\varepsilon = [\text{RT Ln}(1 + 1/C_e)]^2$ ) for adsorbed metal ions on the composite is shown in Fig. 10c. The value of mean free energy,  $E$ , can be calculated as follows:

$$E = \frac{1}{\sqrt{2k_D}} \quad (6)$$

where the mean free energy,  $E$ , of sorption is 2.72 and 2.84 ( $\text{Kj mol}^{-1}$ ), respectively, which is below 8 ( $\text{Kj mol}^{-1}$ ). It indicates that the adsorption process of Pb(II) and Cd(II) ions on the adsorbent involves a physical adsorption mechanism [22].

The maximum adsorption capacity of HAp/NaP was 55.55 mg Pb(II)/g and 40.16 mg Cd(II)/g (see Table 4). The

**Fig. 10** a Freundlich, b Temkin, and c Dubinin–Radushkevich isotherms of metal ions on HAp/NaP



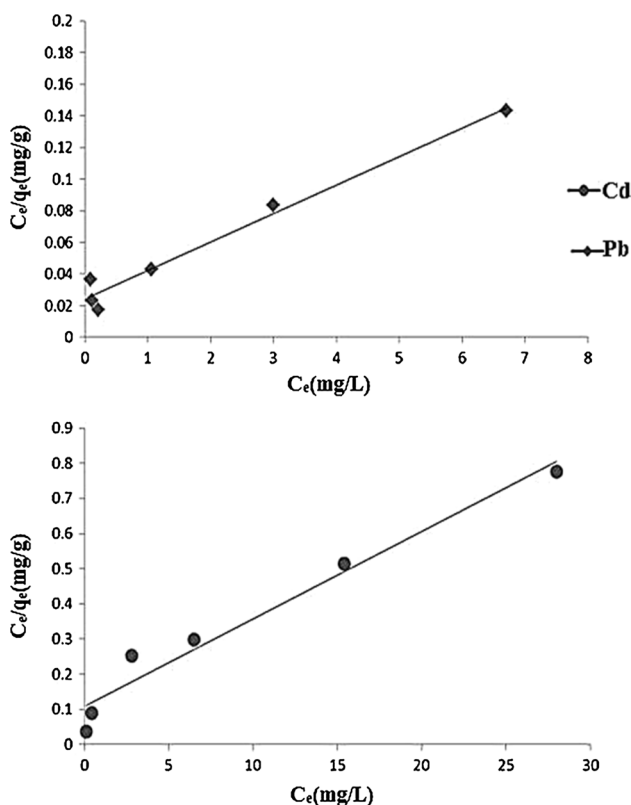


Fig. 11 Langmuir isotherms of Pb(II) and Cd(II) ions on HAp/NaP

adsorption capacity of HAp/NaP for Pb(II) and Cd(II) is compared with other adsorbents (Tables 5, 6). The value of Pb(II) and Cd(II) uptake by HAp/NaP found in this work is significantly higher than that of other adsorbents. From Tables 5 and 6, it can be realized that HAp/NaP is an efficient adsorbent for the uptake of Pb(II) and Cd(II) from aqueous solution.

Adsorption kinetics

The kinetic studies of sorption process were carried out to determine the equilibrium time and rate mechanism

of adsorption. In order to estimate the rate constant, the pseudo-second-order kinetic model was considered. The pseudo-second-order equation can be written as follows [63]:

$$\left(\frac{t}{q_t}\right) = \frac{1}{k_2 q_e^2} + \frac{1}{q_e}(t) \tag{7}$$

where  $k_2$  is the rate constant of second-order rate adsorption in  $(g\ mg^{-1}\ min^{-1})$ . The value of  $q_e$  and  $k_2$  can be determined from the slope and intercept of the plot obtained by plotting  $\frac{t}{q_t}$  versus  $t$ . Figure 12 shows the plot of kinetic model for adsorption of Pb(II) and Cd(II) on HAp/NaP nanocomposite. The high correlation coefficient ( $R^2 = 0.999$ ) for both Pb(II) and Cd(II) indicated the pseudo-second model which perfectly fitted the experimental data.

Desorption experiment

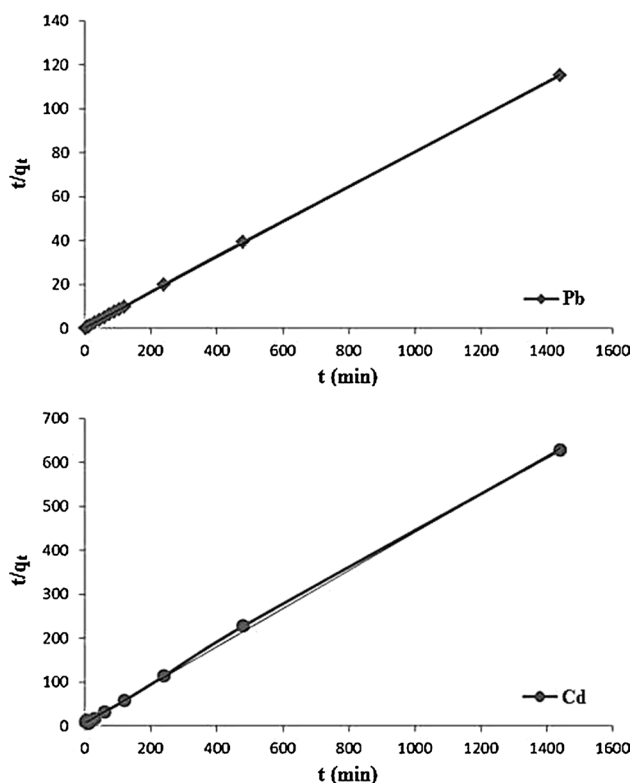
Desorption studies were done by using lead(II) and cadmium(II) adsorbed on HAp/NaP nanocomposite. 2 g/L of HAp/NaP sorbent was regenerated in 25 mL of lead(II) and cadmium(II) solutions (25 mg/L and 5 mg/L respectively) with using optimized pH (5 for Pb(II) and 8 for Cd(II)). The used optimized pH for the investigated reactions were 5 for Pb(II) and 8 for Cd(II). After the equilibration, the filtrate of the reaction was measured for dose of lead(II) and cadmium(II). As a sequence, ion-adsorbed nanocomposite samples were added into 25 mL of 0.01 N  $H_2SO_4$  for 1 h, and then, the filtrate was measured for lead(II) and cadmium(II) content. For a second time, this adsorbent floated in desired solution of lead(II) and cadmium(II) for 2 h, and the concentration of residue ions was determined. This cycle was repeated 10 times. The amount of ions removed from the solution is given in Fig. 13. As shown in Fig. 13, the results indicated that the desorption of the adsorbed lead(II) and cadmium(II) in acid solution resulted about 70 and 64 % for lead(II) and cadmium(II), respectively, after 10 times sorption/desorption experiment. The results showed that the high

Table 5 Comparison of Pb(II) adsorption capacities of different adsorbents

No	Adsorbent	Adsorption capacity (mg/g)	Reference
1	Chicken feathers	8.63	[44]
2	Kaolinite clay	2.35	[45]
3	Commercial activated carbon, bamboo dust carbon	5.95, 2.15	[46]
4	Crab shell, arca shell	19.83, 18.33	[47]
5	Activated carbon powder	20.7	[48]
6	MoringaoleiferaBark	34.6	[49]
7	Activated alumina-supported iron oxide	35.45	[50]
8	Zeolite 3A	14.641	[51]
9	Calcite	19.92	[52]
10	Activated carbon prepared from Phaseolus aureus hulls	28.8	[53]

**Table 6** Comparison of Cd(II) adsorption capacities of different adsorbents

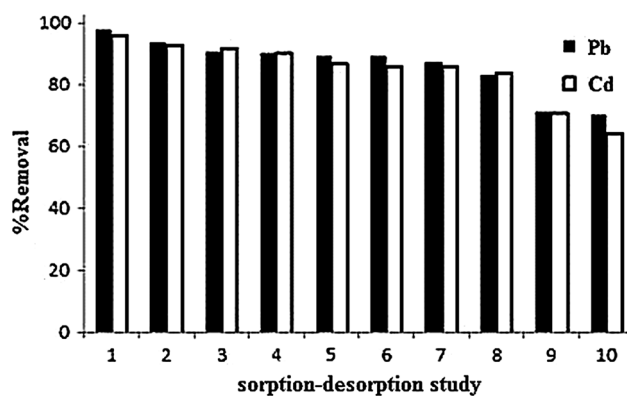
No	Adsorbent	Adsorption capacity (mg/g)	References
1	Calcite	18.52	[52]
2	Old newspaper	1.4405	[54]
3	Sugarcane Bagasse	6.79	[55]
4	Husk of Melon ( <i>Citrulluslanatus</i> ) Seed	7.81	[56]
5	Algerian Bentonite	13.17	[57]
6	KAO.1, MKB	7.407, 9.174	[58]
7	Hazelnut shell, Hazelnut shell ash	0.039, 0.004	[59]
8	Corncob	5.09	[60]
9	Grape stalk	27.88	[61]
10	Psidiumguvajaval/leaf powder	31.15	[62]

**Fig. 12** Pseudo-second-order sorption kinetics of Pb(II) and Cd(II) onto HAp/NaP

desorption values were observed, and this adsorption of lead(II) or cadmium(II) ions on the investigated nanocomposite was physical. Hence, recovery of the adsorbent is very easy. This result is according to the E value calculated by D-R isotherm in 3.6.7 section.

### Biological studies

The *in vitro* antibacterial activities of HAP nanopowder and HAP/zeolite (0.5:1, 1:1, and 2:1) were studied with

**Fig. 13** Amount of removal of ions for each experiment

two standard antibacterial drugs, vancomycin and nalidixic acid. The microorganisms used in this study include *B. subtilis* (as Gram-positive bacteria) and *P. aeruginosa* (as Gram-negative bacteria). The results are presented in Table 6. Comparing the biological activity of the HAP nanopowder and HAP/zeolite (0.5:1, 1:1, and 2:1) with standard drugs indicates that incorporated nano-HAP to composite shows more inhibition on bacterial growth. It seems that the aggregation effect is very significant in antibacterial activity of nano-hydroxyapatite that decreases with incorporated of zeolite. It is apparent that toxicity toward Gram-positive bacteria is more than Gram-negative strains, and because peptidoglycan is negatively charged, HAP nanoparticles are positively charged [21]. The reason is the difference in the structure of the cell wall. The walls of Gram-negative cells are more complex than those of Gram-positive cells, and lipopolysaccharides form an outer lipid membrane and contribute to the complex antigenic specificity of Gram-negative cells. Also, we know that some bacteria such as *P. aeruginosa* are a group of resistant microorganism to many standard drugs, and they were found to have no activity against it. Then, it is interesting that *P. aeruginosa* was inhibited by these nanocomposites [64] (Table 7).

**Table 7** Antibacterial activity data of HAp nanopowder and HAp/zeolite

Compounds	Inhibition zone (mm)	
	<i>B. subtilis</i> (Gram positive)	<i>S. aeruginosa</i> (Gram negative)
HAp	14	10
HAp/zeolite (0.5:1)	18	12
HAp/zeolite (1:1)	21	13
HAp/zeolite (2:1)	22	15
Vancomycine	23	No activity
Nalidixic acid	22	No activity

## Conclusion

The nanocomposite of HAp/NaP was prepared and characterized using various methods such as XRD, FT-IR, TGA/DTA, BET, SEM, and EDAX. The results showed that with the addition of HAp-to-NaP zeolite, the nanosize crystals of the synthesized HAp became more dispersed onto the zeolite external surface and/or incorporated within the zeolite channels and pores. It did not cause a significant reduction in the zeolite microporosity and crystallinity or collapse of the zeolite crystal structure. The nanocomposite of HAp/NaP showed a good efficiency in Pb(II) and Cd(II) removal from aqueous solution. Optimum dose of adsorbent was found to be 2 g/L, and the adsorption capacity of nanocomposite decreased with increasing pH for the removal of Pb(II), while removal of Cd(II) ions increased with increasing pH from 5 to 8. The effect of temperature on the adsorption of Pb(II) and Cd(II) ions was studied using optimum conditions such as adsorbent dose, pH, contact time, and initial concentration of aqueous solution. It was observed that there was small decrease effect in adsorption by increasing temperature. The effect of initial concentration was studied. It can be seen that the percentage removal of both ions decreases with increase in initial ion concentration. The optimum initial concentration was found to be 25 mg/L for Pb(II) ion and 5 mg/L for Cd(II) ion solution. The adsorption of heavy metal ions on HAp/NaP obeyed a pseudo-second-order kinetic model. The equilibrium adsorption data of Pb(II) were fitted to the Temkin isotherm rather than the other isotherm models, and in case of Cd(II), the equilibrium data were fitted to the Freundlich isotherm model. The D-R isotherm model was also applied to analyze adsorption data. The value of obtained E indicates a physical adsorption mechanism for Pb(II) and Cd(II) on HAp/NaP. Results of antibacterial activity show that HAp/zeolite nanocomposites are active against most common Gram-positive and Gram-negative bacteria making it useful for wastewater treatment.

**Acknowledgments** Thanks are due to the Iranian Nanotechnology Initiative and the Research Council of Arak University of Technology and Center of Excellence in the Chemistry Department of Arak University of Technology for supporting this work.

## References

- P. Trivedi, L. Axe, Environ. Sci. Technol. **34**, 2215 (2000)
- S.T. Ramesh, N. Rameshbabu, R. Gandhimathi, M. Srikanth Kumar, P.V. Nidheesh, Appl. Water Sci. **3**, 105 (2013)
- M.N. Rashed, Environmentalist **21**, 187 (2001)
- P. King, N. Rakesh, S. Beenalahari, Y. Prasanna Kumar, V.S.R.K. Prasad, J. Hazard. Mater. **142**, 340 (2007)
- R. Naseem, S.S. Tahir, Wat. Res. **35**, 3982 (2001)
- Z. Elouear, J. Bouzid, N. Boujelben, M. Feki, F. Jamoussi, A. Montiel, J. Hazard. Mater. **156**, 412 (2008)
- G. Crini, Prog. Polym. Sci. **30**, 38 (2005)
- G. Crini, Bioresour. Technol. **97**, 1061 (2006)
- F. Bouhamed, Z. Elouear, J. Bouzid, J. Taiwan Inst. Chem. Eng. **43**, 741 (2012)
- Ch. Baerlocher and L.B. McCusker, Database of Zeolite Structures: <http://www.iza-structure.org/databases/>
- T. Motsi, N.A. Rowson, M.J.H. Simmons, Int. J. Miner. Process. **92**, 42 (2009)
- A. Banerjee, A. Bandyopadhyay, S. Bose, Mater Sci Eng C. **27**, 729 (2007)
- V.D.B.C. Dasireddy, S. Singh, H.B. Friedrich, Appl. Catal. A **421–422**, 58–69 (2012)
- S. Wang, Y. Lei, Y. Zhang, J. Tang, G. Shen, R. Yu, Anal. Biochem. **398**, 191 (2010)
- S. Smičiklas, I. Dimović, M. Plečaš, Mitric. Water Research. **40**, 2267 (2006)
- S.T. Ramesh, N. Rameshbabu, R. Gandhimathi, P.V. Nidheesh, M. Srikanth-Kumar, Appl Water Sci. **2**, 187 (2012)
- A. Corami, S. Mignardi, V. Ferrini, J. Hazard. Mater. **146**, 164 (2007)
- C.S. Sundaram, N. Viswanathan, S. Meenakshi, J. Hazard. Mater. **155**, 206 (2008)
- K. Lina, J. Pana, Y. Chena, R. Chenga, X. Xua, J. Hazard. Mater. **161**, 231 (2009)
- H.S. Ragab, F.A. Ibrahim, A.A. Al-Ghamdi, F. El-Tantawy, F. Yakuphanoglu, J. Pharm. Biol. Sci. **9**, 77 (2014)
- J.J. Hwang, T.W. Ma, Mater. Chem. Phys. **136**, 613 (2012)
- Y. Zhan, J. Lin, J. Li, Environ Sci Pollut Res. **20**, 2512 (2013)
- M. Sadeghi, S.L. Sharifi, H. Hatami, Int. J. NanoDimens. **5**, 91 (2014)
- Y. Wang, S. Zhang, K. Wei, N. Zhao, J. Chen, X. Wang, Mater. Lett. **60**, 1484 (2006)
- Y. Xiaolin, T. Shengrui, G. Maofa, Z. Junchao, Carbohydr. Polym. **92**, 269 (2013)
- A.H. Alwash, A.Z. Abdullah, N. Ismail, J. Hazard. Mater. **233–234**, 184 (2012)
- M. Abecassis-Wolfovich, R. Jothiramalingam, M.V. Landau, M. Herskowitz, B. Viswanathan, T.K. Varadarajan, Appl. Catal. B: Environ. **59**, 91 (2005)
- S. Hansen, U. Hakansson, L. Faelth, Acta Crystallogr. C **46**, 1361 (1990)
- H. El Feki, J.M. Savariault, A. Ben Salah, J Alloys Compounds. **287**, 114 (1999)
- Z. Huo, X. Xu, Z. Lü, J. Song, M. He, Z. Li, Q. Wang, L. Yan, Microporous Mesoporous Mater. **158**, 137 (2012)
- K.J. Balkus, A.G. Gabrielov, J. Inclusion Phenom. Mol. Recognition Chem. **21**, 159 (1995)

32. R. Szostak, *Molecular Sieves: Principles of Synthesis and Identification* (Van Nostrand Reinhold, New York, 1989)
33. A. Corma, *Chem. Rev.* **97**, 2373 (1997)
34. G. Cruciani, *J. Phys. Chem. Solids* **67**, 1973 (2006)
35. D.W. Breck, Zeolite molecular sieves: structure, chemistry and use. *J. Chromatogr. Sci.* (1974). doi:10.1093/chromsci/13.4.18A-c
36. S. Singh, S.B. Jonnalagadda, *Bull. Chem. Soc. Ethiop.* **27**, 57 (2013)
37. M. Zendejdel, H. Khanmohamadi, M. Mokhtari, *J. Chin. Chem. Soc.* **57**, 205 (2010)
38. M. Răţoi, L. Bulgariu, M. Macoveanu, Removal of lead from aqueous solutions by adsorption using sphagnum moss peat, *Chem. Bull. "POLITEHNICA" Univ. (Timişoara)*. **53**, 1 (2008)
39. M.A.O. Badmus, T.O.K. Audu, B.U. Anyata, *Turkish J. Eng. Env. Sci.* **31**, 251 (2007)
40. D. Tilaki, R. Ali, *Ecology* **8B**, 8 (2003)
41. R. Zhu, R. Yu, J. Yao, D. Mao, Ch. Xing, D. Wang, *Catal. Today* **139**, 94 (2008)
42. M. Islam, R.K. Patel, *J. Hazardous Materials*. **143**, 303 (2007)
43. Y.S. Ho, J.F. Porter, G. McKay, *Water Air Soil Pollut.* **141**, 1 (2002)
44. G. De la Rosa, HE. Reynel-Avila, A. Bonilla-Petriciolet, I. Cano-Rodríguez, C. Velasco-Santos, AL. Martínez-Hernández, *Int. J. Chem Biol Eng.* **1**, 185 (2008)
45. M.Q. Jiang, X.Y. Jin, X.Q. Lu, Z.L. Chen, *Desalination*. **252**, 33 (2010)
46. N. Kannan, T. Veemaraj, *Electron J Environ Agric Food Chem.* **6**, 247 (2009)
47. S. Dahiya, R.M. Tripathi, A.G. Hegde, *Bioresour. Tech.* **99**, 179 (2007)
48. J.T. Matheickal, Q. Yu, Proceedings of the 10th national convention of Royal Australian Chemical Institute. Adelaide, Australia, (1996)
49. D.H.K. Reddy, K. Seshiah, A.V.R. Reddy, M. Madhava-Rao, M.C. Wang, *J. Hazard. Mater.* **174**, 831 (2010)
50. Y.H. Huang, C.L. Hsueh, C.P. Huang, L.C. Su, C.Y. Chen, *Sep. Purif. Technol.* **55**, 23 (2007)
51. W. Rondón, D. Freire, Z. de Benzo, A.B. Sifontes, Y. González, M. Valero, J.L. Brito, *Am J Anal Chem.* **4**, 584 (2013)
52. Ö. Yavuz, R. Guzel, F. Aydin, I. Tegin, R. Ziyadanogullari, *Polish J. Environ. Stud.* **16**, 467 (2007)
53. M.M. Rao, D.K. Ramana, K. Seshiah, M.C. Wang, C.S.W. Chang, *J. Hazard. Mater.* **166**, 1006 (2009)
54. M.E. Ossman, M.S. Mansour, *Int. J. Ind. Chem.* **4**, 1 (2013)
55. S.C. Ibrahim, M.A.K.M. Hanafiah, M.Z.A. Yahya, *Am-Euras. J. Agric Environ. Sci.* **1**, 179 (2006)
56. A.A. Giwa, I.A. Bello, M.A. Oladipo, D.O. Adeoye, *Int J. Basic Appl Sci* **2**, 110 (2013)
57. M. Barkat, S. Chegrouche, A. Mellah, B. Bensmain, D. Nibou, M. Boufatit, *J. Surface Eng Mater Adv Technol* **4**, 210 (2014)
58. J.S. Essomba, J.N. Nsami, P.D.B. Belibi, G.M. Tagne, J.K. Mbadcam, *Pure Appl Chem Sci.* **2**, 11 (2014)
59. H.A. Jamali, A.H. Mahvi, Sh Nazmara, *World Appl. Sci. J.* **5**, 16 (2009)
60. R.L. Ramos, L.A.B. Jacome, I.A. Rodriguez, *Sep. Puri. Technol.* **4**, 41 (2005)
61. M. Martínez, N. Miralles, S. Hidalgo, I. Villaescusa, J. Poch, *J. Hazard. Mater.* **B133**, 203 (2006)
62. K.S. Rao, S. Anand, P. Venkateswarlu, Psidiumguvajaval leaf powder. *Adsorpt Sci Technol* **28**, 163 (2010)
63. Y.S. Ho, G. McKay, *Process Biochem.* **34**, 451 (1999)
64. R. Juan-Luis, F. Alian, *Pseudomonas, Virulence and Gene Regulation*, 2nd edn. (Springer, New York, 2007)